JOURNAL OF Materials CHEMISTRY

Formation and structural characterisation of ammonium vanadyl phosphates prepared by solid state reactions of vanadyl(IV) phosphates in the presence of ammonia

Andreas Martin,*[a] Lutz Wilde,[a] Ursula Steinike,[a]

[a]*Institut für Angewandte Chemie Berlin-Adlershof e.V., Richard-Willstätter-Str. 12, D-12489 Berlin, Germany*

Received 26th April 2000, Accepted 30th June 2000
First published as an Advanced Article on the web 9th August 2000

The structural transformation of various vanadyl(IV) phosphates into vanadium oxide-containing crystalline $(NH_4)_2(VO)_3(P_2O_7)_2$ in the presence of ammonia-containing gas flows and under ammoxidation of toluene reaction conditions has been investigated using a coupled hot stage XRD and on-line GC apparatus. Two different types of crystalline layered NH_4^+-containing vanadium phosphates were generated as intermediate phases during the formation process: (i) $NH_4VOPO_4{\cdot}nH_2O$, $n=0.5$, 2, 4, a kind of intercalation compound formed between 293 and 390 K, and (ii) β-$(NH_4)_2(VO)_3(P_2O_7)_2$, observed during a period where the temperature was held constant at 713 K. Besides the formation of these crystalline intermediates, the generation of X-ray amorphous states was noted. The final product, consisting of distorted ammonium vanadyl(IV) pyrophosphate [α-$(NH_4)_2(VO)_3(P_2O_7)_2$], additionally contains various amounts of X-ray amorphous vanadium oxides. The transformation process is discussed on the basis of the precursor structures. Measurable catalytic activity was not observed until the formation of β-$(NH_4)_2(VO)_3(P_2O_7)_2$. Increased catalytic activity is associated with the formation of α-$(NH_4)_2(VO)_3(P_2O_7)_2$ and the generation of vanadium oxide co-phases. The *in situ* XRD data obtained during the phase transformation and the evaluation of the simultaneously-received data on catalytic performance at different transformation stages provide a more detailed insight into the formation of an effective catalyst and its catalytic performance from the position of the bulk structure.

Vanadium phosphates (VPO) are well known as effective catalysts for the partial oxidation of *n*-butane to maleic anhydride (*e.g.* ref. 1–3). Vanadyl(IV) pyrophosphate [$(VO)_2P_2O_7$] is the most interesting material in this group of solids as it is considered to be the active and selective crystalline phase of such catalytic systems. $(VO)_2P_2O_7$ is mostly generated from a precursor compound (*e.g.* $VOHPO_4{\cdot}0.5H_2O$) during a topotactic transformation process.[1,4] VPO solids have also been successfully employed as selective catalysts in the heterogeneous catalytic ammoxidation of methyl aromatics and methyl heteroaromatics (*e.g.* ref. 5–7, and references therein).

Recently, it was found that ammonium-containing vanadyl(IV) pyrophosphates [*e.g.* $(NH_4)_2(VO)_3(P_2O_7)_2$; V/P = 0.75] are formed from vanadyl(V) monophosphates ($VOPO_4$; V/P = 1),[8,9] vanadyl(IV) hydrogen phosphates ($VOHPO_4{\cdot}nH_2O$; $n=0$, 0.5, 2, 4; V/P = 1)[10,11] and from vanadyl(IV) monophosphates [$(VO)_3(PO_4)_2{\cdot}nH_2O$; $n=7$, 9; V/P = 1.5],[12] respectively, under ammoxidation conditions (methyl aromatics–ammonia–air–water vapour feed at temperatures of about 670 K for some hours). A crystalline $(NH_4)_2(VO)_3(P_2O_7)_2$ (AVP) phase was always detected by X-ray diffraction (XRD) analysis after phase transformation of the precursor materials, both during the catalytic reaction or precursor pretreatment in the presence of air, water vapour and ammonia only. But only three-quarters and half, respectively, of the initial vanadium contents of the different precursor compounds are located in the identified AVP solids. Therefore, the existence of an additional vanadium-rich phase in various portions seemed to be very likely and could be assumed from the stoichiometry of the precursor–catalyst transformation [V/P ratio of the precursor (1 and 1.5) in comparison to the one of the crystalline AVPs (0.75)]. This additional phase is somewhat X-ray amorphous; however, dependent upon its concentration X-ray observation partly succeeded.[9,12] Potentiometric titration measurements of transformation products revealed a vanadium valence state of approximately 4.12 (starting from mono- and hydrogen phosphates with V/P = 1) to 4.25 (starting from monophosphates with V/P = 1.5). Thus, from these investigations, it also seemed likely that a vanadium-rich co-phase accounts for the remainder of the vanadium content of the precursor compound and represents a mixed-valent $V^{IV/V}$ oxide phase (V_xO_y) due to the vanadium valence state of 4.0 in the crystalline AVP component. Interestingly, the use of precursor compounds with V/P <1.0 [V/P = 0.5; $(NH_4)_2VOP_2O_7$, $VO(H_2PO_4)_2$][13] or >1.5 [V/P = 2; $(NH_4)(VO_2)_2PO_4{\cdot}3H_2O$][14] does not lead to the formation of AVP under the aforementioned conditions. Additionally, the well known $(VO)_2P_2O_7$ compound does not form AVP during the ammoxidation reaction either.[8]

Obviously, the solids generated in such precursor transformations consist of two components, AVP and V_xO_y. These materials are referred to in the following as AVP_{gen} to distinguish them from the pure as-synthesised AVP compound, which is denoted AVP_{syn}. All studied AVP_{gen} catalysts showed a much higher catalytic activity in the ammoxidation of toluene, used as model reaction, than AVP_{syn}, which was nearly inactive. Therefore, the catalytic activity must arise from the mixed-valent $V^{IV/V}$ oxide phase and this is a further proof of its existence and effect. It is well known that various vanadium oxides are very active but somewhat unselective ammoxidation catalysts.[15] Grasselli and Burrington suggest that it is crucial in oxidation catalysis to separate the active centres to prevent total oxidation and thus enhance selectivity.[16] Actually, the observation of spatially separated V_xO_y proportions using Raman spectroscopy succeeded recently, indicating V_2O_5.[17] However, this means that the AVP structure probably only acts as a matrix for the catalytically active V_xO_y phase. In general, the catalytic activity is improved with an enhanced V_xO_y content in the catalyst and an increased V/P ratio, both in the bulk and on the surface. The highest catalytic activity in the

 DOI: 10.1039/b003318i

series of the AVP_{gen} catalysts was observed using catalysts generated from vanadyl(IV) monophosphate precursor compounds with a V/P ratio of 1.5.[12] Nevertheless, significant differences in the catalytic activity were also observed with catalysts generated from precursor compounds with the same V/P ratio [$VOPO_4{\cdot}2H_2O$ and $VOHPO_4{\cdot}nH_2O$ (*e.g.* $n=0.5$); V/P = 1]. The $VOPO_4{\cdot}2H_2O$-derived catalyst showed a significantly increased activity. This effect could be due to the different vanadium oxidation state of the precursor compounds, probably leading to easier formation of higher valent V_xO_y species in the case of the V(V) precursor. In fact, the observation of crystalline V_2O_5 proportions by XRD after phase transformation confirmed these ideas.[9]

The knowledge of the composition and structure of catalysts on the surface and in the bulk, as well as reactant–catalyst interactions is crucial to a fundamental understanding of the chemistry occurring in heterogeneously catalysed reactions.[18,19] Additionally, such results are essential for the understanding and explanation of catalytic processes. In redox reactions (*e.g.* ammoxidation of methyl aromatics), the electronic configuration and the morphology of oxides are important in determining their catalytic activity and product selectivities. *In situ* methods can help to shed more light onto the characterisation of the working state of catalysts, as well as the feed–solid interactions.[20]

The purpose of the present study was to investigate the course of the transformation process of different vanadyl(IV) phosphate precursor compounds by an *in situ* XRD technique and to identify the intermediate phases and their influence on the generation, composition and structure of a final catalyst. Simultaneously, the structural investigation of the phase transformation was accompanied by a time-resolved gas chromatographical analysis of the product stream to compare the structural and catalytic properties of the solids during different transformation steps. Various vanadyl(IV) hydrogen phosphates ($VOHPO_4{\cdot}nH_2O$; $n=0$, 0.5, 2, 4; V/P = 1) and a vanadyl(IV) monophosphate [β-$(VO)_3(PO_4)_2{\cdot}6H_2O$; V/P = 1.5] were selected as precursor compounds.

Experimental

Synthesis of the precursor phases

The vanadyl(IV) phosphate precursor compounds were synthesised according to standard methods. The hydrothermal synthesis of $VOHPO_4{\cdot}0.5H_2O$, $VOHPO_4{\cdot}2H_2O$, $VOHPO_4{\cdot}4H_2O$ and β-$(VO)_3(PO_4)_2{\cdot}6H_2O$ was carried out as proposed by Fratzky *et al.*[21] 45.3 g of V_2O_5 were dissolved in a solution containing 36 ml H_3PO_4 (85%), 90 ml of distilled water and 43.5 g $(COOH)_2{\cdot}2H_2O$ at 353 K, and kept at this temperature for 12 h. After cooling, distilled water was added to a total weight of 220 g, corresponding to a vanadium concentration of 3.13 mol l^{-1}. This parent solution was further diluted with distilled water to a defined vanadium concentration, placed into a Teflon sealed autoclave and kept for 14 days at temperatures of up to *ca.* 423 K. Table 1 summarises the exact reaction conditions employed. $VOHPO_4$ was synthesised by reduction of β-$VOPO_4$ with ethylene glycol monoethyl ether (bp = 405 K, heating under reflux for 2 h).[22]

Pure $(NH_4)_2(VO)_3(P_2O_7)_2$ (AVP_{syn}) was obtained by heating of a mixture of V_2O_5 and $(NH_4)_2HPO_4$ (molar ratio of V : P : N = 1 : 8 : 16) to *ca.* 400 K under air for at least 2 h.[10] The light green powder was washed with distilled water and dried under air.

Table 1 Reaction conditions for the synthesis of various vanadyl(IV) phosphate precursor compounds

Precursor compound	$c_{vanadium}$/mol l^{-1}	T/K	$p_{nitrogen}$/bar
$VOHPO_4{\cdot}0.5H_2O$	0.782	413	—
$VOHPO_4{\cdot}2H_2O$	1.565	373	—
$VOHPO_4{\cdot}4H_2O$	1.565	323	—
β-$(VO)_3(PO_4)_2{\cdot}6H_2O$	0.391	393	100

Table 2 Abbreviations used for the various AVP_{gen} solids prepared and the respective precursor compounds employed

Sample	Precursor compound
AVP_{gen0}	$VOHPO_4$
$AVP_{gen0.5}$	$VOHPO_4{\cdot}0.5H_2O$
AVP_{gen2}	$VOHPO_4{\cdot}2H_2O$ (α-phase)
AVP_{gen4}	$VOHPO_4{\cdot}4H_2O$
AVP_{gen6H}	β-$(VO)_3(PO_4)_2{\cdot}6H_2O$

Table 2 lists the precursor compounds used, as well as abbreviations for the AVP_{gen} specimens resulting after phase transformation.

Structure of the precursor phases

The crystal structures of the precursor phases differ significantly, as depicted in Fig. 1. The crystal water-containing vanadium hydrogen phosphates $VOHPO_4{\cdot}nH_2O$ [$n=0.5$, 2(α), 4] form layered structures that are held together *via* hydrogen bonds. The crystal structure of $VOHPO_4{\cdot}0.5H_2O$ is made up of layers perpendicular to the *c*-axis, which themselves consist of pairs of face-sharing VO_6 octahedra.[23] The units are interconnected by PO_3–OH tetrahedra. Each water molecule is covalently bound to two vanadium atoms, thus having a

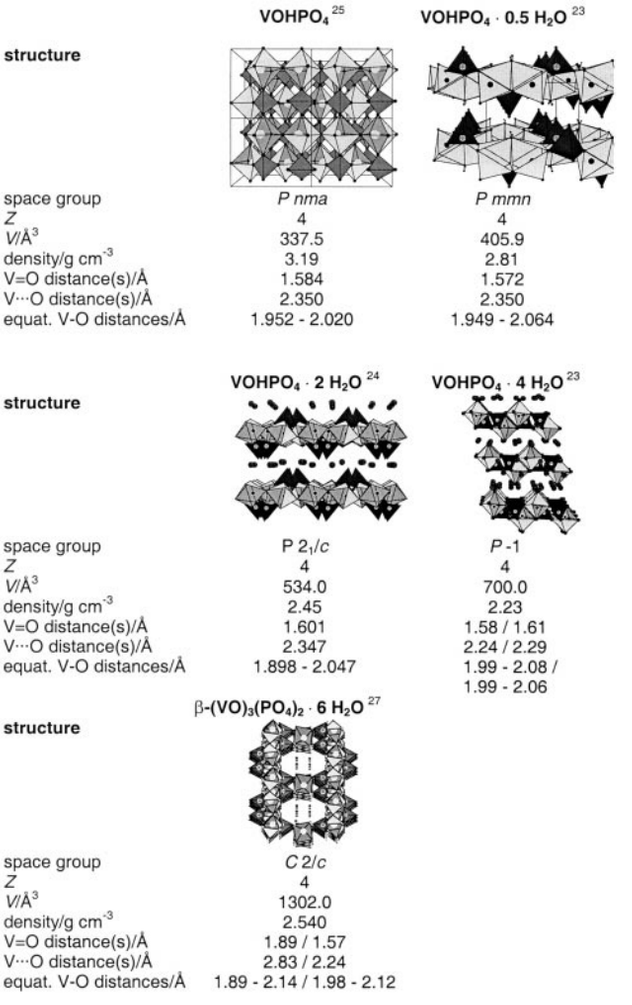

Fig. 1 Comparison of the structures of the precursors and their structural data.

relatively high binding energy. The unshared hydroxyl groups of the PO_3–OH tetrahedra rise up into the interlayer space.

The structure of $VOHPO_4{\cdot}4H_2O$ is closely related to that of $VOHPO_4{\cdot}0.5H_2O$.[23] It consists of double chains of alternating PO_3–OH and $VO_4(H_2O)_2$ units. These double chains form sheets parallel to the *c*-direction. Water molecules that are not covalently bound are located between these sheets. A network of hydrogen bonds connects the sheets to each other. As Leonowicz *et al.* showed, the structure of $VOHPO_4{\cdot}4H_2O$ is~easily converted into that of $VOHPO_4{\cdot}0.5H_2O$, with theoccurrence of β-$VOHPO_4{\cdot}2H_2O$ as an intermediate phase.[23]

The layers within the structure of $VOHPO_4{\cdot}2H_2O$ (α-phase) which are perpendicular to the *a*-direction consist of VO_6 octahedra chains running parallel to the *b*-axis.[24] The chains are linked together by PO_3–OH tetrahedra. Half of the water molecules are covalently bound to vanadium atoms, the other half are located between the layers.

The distances between the layers in the $VOHPO_4{\cdot}nH_2O$ precursor compounds are *ca.* 5.7 ($n=0.5$), 7.6 ($n=2$) and 8.2 Å ($n=4$).

In contrast, anhydrous $VOHPO_4$ crystallises in a three-dimensional network consisting of VO_6 octahedra chains running parallel to the *a*-direction.[25] The chains are interconnected by PO_4(H) tetrahedra. The compound is isostructural to β-$VOPO_4$.[26] Furthermore, $VOHPO_4$ does not show any unshared hydroxyl groups. The hydrogen atom is believed to be disordered.

The precursor β-$(VO)_3(PO_4)_2{\cdot}6H_2O$ stands out for its tunnel-like structure. The two independent V atoms form chains of VO_6 octahedra, each running parallel to crystallographic directions. Both types of chains are connected to each other by PO_4 tetrahedra. This finally results in the formation of ellipsoidal tunnels (diameters of about 7 and 10 Å) that run parallel to the *c*-axis. Two thirds of the water molecules are covalently bound to both V atoms, the remainder are located within the tunnels and are connected to the structure *via* hydrogen bonds.

In situ XRD measurements

The precursor transformation and catalytic experiments followed by *in situ* XRD were carried out in an XRK reactor chamber (Anton Paar GmbH, Austria) that was used as a catalytic flow reactor (Fig. 2).[27] A standard gas/liquid supply system with mass flow controllers and saturators was assembled for introducing the reactant flow. The product stream was analysed on line using a capillary gas chromatograph (Shimadzu GC-17A; column: FS-SE-54CB) and a flame ionisation detector. The VPO precursor compounds used for the experiments (*ca.* 150 mg) were powdered, with an average particle diameter of about 7 μm. The solids were placed on a sieve-like sample holder made of Inconel steel. The reaction mixture passed through the precursor/catalyst powder and left the chamber for analysis *via* a small tube connected to the sieve (Fig. 2). A thermocouple was directly

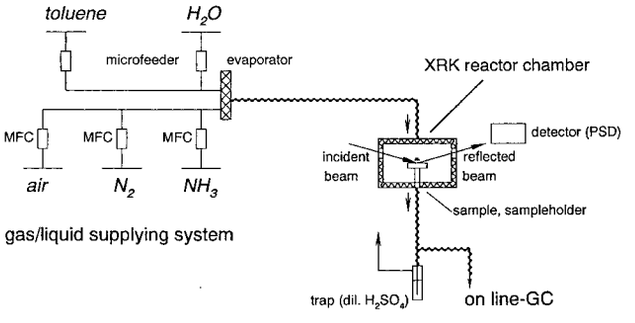

Fig. 2 Scheme of the *in situ* XRD/catalytic reactor set-up.

located next to the sample which could be heated from room temperature up to 1173 K. The XRK reactor chamber was connected to a thermostat, keeping the temperature of the outer reactor chamber jacket above 393 K to avoid condensation of water or organic vapour. The actual *in situ* XRD measurements were carried out using a URD6 diffractometer (FPM-Seifert, Germany; Bragg–Brentano geometry, Cu-Kα) equipped with a PSD as detector (Stoe, Germany). The intensity yield was rather low due to absorption, since the X-rays had to pass through Capton foils in the incident as well as in the reflected beam. The feed composition used was: toluene : ammonia : air : water vapour = 1 : 4.5 : 32 : 24 (molar ratio). The following general temperature regime was adopted: (i) the sample was heated to 393 K under an air–ammonia flow, (ii) water and toluene vapour were added to this mixture above 393 K to prevent condensation, (iii) the sample was further heated to 713 K at a rate of 2.5 K min^{-1} and (iv) the final temperature was then maintained for about 5 h. The composition of the reactor outlet stream was automatically analysed in 10 min steps to check toluene conversion and benzonitrile formation. The selected *in situ* reaction conditions follow the usually used and recently described *ex situ* conditions,[11–13] but there are also some considerable differences (amount of catalyst sample, catalyst particle size). Blank tests showed that the hot metallic surfaces of the XRK reactor chamber (sample holder, heater) do not act as catalysts. Also, a gas phase reaction does not take place.

Characterisation

Characterisation of the parent samples and the products after the transformation were carried out at room temperature by means of XRD and measurements of the extended X-ray absorption fine structure (EXAFS). Additionally, the formation of NH_4^+-containing specimens was monitored by FTIR spectroscopy.

The XRD patterns were recorded using a STADI P (Stoe, Germany) set-up (Debye–Scherrer geometry, Ge primary monochromator, Cu-$K\alpha_1$). Data interpretation was carried out using the X-POW software (Stoe, Germany) and the database of the International Centre for Diffraction Data (ICDD). The following PDF files were used for comparison: $VOHPO_4$ (PDF 48-1158),[25] $VOHPO_4{\cdot}0.5H_2O$ (PDF 37-0269), α-$VOHPO_4{\cdot}2H_2O$ (PDF 44-0598), $VOHPO_4{\cdot}4H_2O$ (PDF 41-0106), β-$(VO)_3(PO_4)_2{\cdot}6H_2O$ (submitted to ICDD) and α-$(NH_4)_2(VO)_3(P_2O_7)_2$ (PDF 47-804). Recently, the structure of β-$(VO)_3(PO_4)_2{\cdot}6H_2O$ was investigated in detail, as described in ref. 27.

The thermal behaviour of AVP_{syn} and $AVP_{gen0.5}$ in N_2 and air, respectively, was investigated by *in situ* XRD analyses in a Guinier–Lenné camera (Nonius, The Netherlands) up to 730 K (heating rate $\beta=1$ K min^{-1}) as well as by thermal analysis using TG-DTA equipment (SETARAM with TAG 24-16; heating rate $\beta=5$ K min^{-1}, sample weight: 10–34 mg). The liberated gases were detected by mass spectrometry (Balzers QMS 421, MID mode).

The EXAFS measurements were carried out at the E4 beamline at Hasylab (DESY, Hamburg). The samples (optimum thickness of about 150 μm) were placed onto polypropene foils using a silk screen printing method.[28] The measurements were taken at the V K-edge ($E=5.465$ keV), scanning equidistant in the k-room.

The infrared spectra of the samples were recorded with a Bruker IFS 66 FTIR spectrophotometer, with 2 mg of sample powder diluted in 400 mg of KBr and pressed into 20 mm o.d. wafers. For each spectrum, 100 scans were accumulated at 2 cm^{-1} resolution.

Results and discussion

In situ XRD observation of the formation of ammonium vanadyl(IV) phosphate catalysts

Fig. 3a and 4a show typical *in situ* XRD pattern series for the generation of AVP_{gen} catalysts using the precursor compounds $VOHPO_4{\cdot}0.5H_2O$ and $VOHPO_4{\cdot}4H_2O$, respectively, under the conditions of the ammoxidation reaction. Figs. 3b and 4b display the simultaneously recorded GC analysis data for the reactant, toluene, and the onset of benzonitrile formation.

The generation of an AVP_{gen} solid from a defined precursor phase was generally observed on reaching the final temperature of *ca.* 713 K. Table 3 lists the detected intermediate phases appearing during the formation of the final AVP_{gen0}, $AVP_{gen0.5}$, AVP_{gen2}, AVP_{gen4} and AVP_{gen6H} solids and their crystalline compositions. In general, intermediate phases existing at temperatures below 500 K are denoted X1 and those appearing at higher temperatures, or during the constant temperature period, are labelled as X2. Besides several crystalline intermediate phases, some intermediate states seem to be X-ray amorphous (in the cases of AVP_{gen2}, AVP_{gen4} and AVP_{gen6H} formation). The results presented in Table 3 clearly demonstrate a different formation mechanism depending on the structure of the precursor compound. It seems very likely that nearly all intermediate phases consist of NH_4^+-containing vanadium phosphates (with the exception of β-$VOPO_4$, $X1_6$ and $X2_0$, although the composition of $X2_0$ is still unknown).

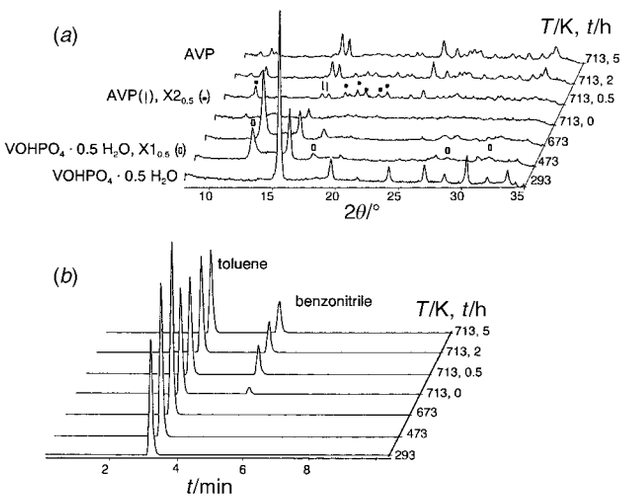

Fig. 3 XRD pattern of (a) the $VOHPO_4{\cdot}0.5H_2O$ to $AVP_{gen0.5}$ transformation process and (b) gas chromatographic analysis of the product stream as a function of time-on-stream.

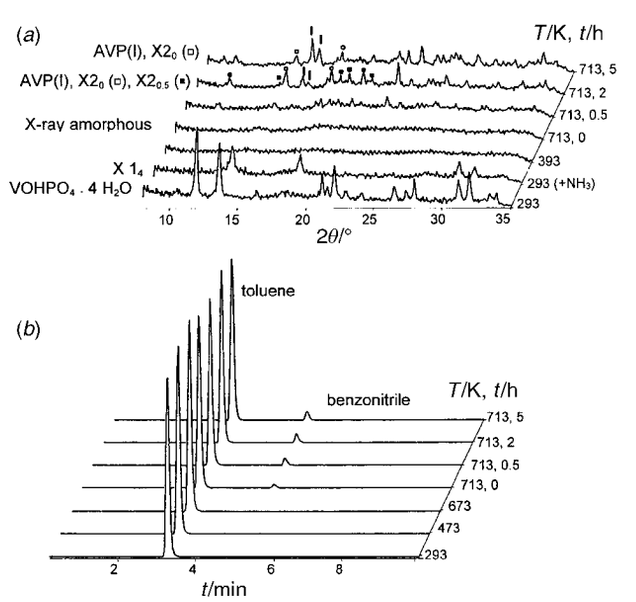

Fig. 4 XRD pattern of (a) the $VOHPO_4{\cdot}4H_2O$ to AVP_{gen4} transformation process and (b) gas chromatographic analysis of the product stream as a function of time-on-stream.

In a first transformation step, the layered V(IV) hydrogen phosphates $VOHPO_4{\cdot}nH_2O$ ($n=0.5$, 2 (α-phase), 4) were partly or completely transformed into ammonium ion-containing intermediates. The wider the layer distance, the lower the temperatures needed for reaction of ammonia with the P–OH groups and the subsequent formation of ammonium ions. The conversion temperatures are 390 K ($n=0.5$; intermediate phase denoted $X1_{0.5}$), 360 K ($n=2$; $X1_2$) and room temperature ($n=4$; $X1_4$). It is assumed that these intermediates could be assigned to $NH_4VOPO_4{\cdot}0.5H_2O$ for $X1_{0.5}$, $NH_4VOPO_4{\cdot}2H_2O$ for $X1_2$ and $NH_4VOPO_4{\cdot}4H_2O$ for $X1_4$. Table 4 lists the *d*-values of the reflections of these intermediates after cooling down to room temperature. Even if we had not been successful in synthesising and further characterising the intermediates, the reaction of ammonia with the P–OH groups is strongly evidenced by the FTIR measurements (Fig. 5). These spectra show a dramatic decrease in the P–OH vibrations at 686 cm^{-1} and the existence of NH_4^+ vibrations at 1426 cm^{-1} that increase with time-on-stream. Furthermore, the incorporation of ammonia results in a widening of the layer distances. In the case of $VOHPO_4{\cdot}0.5H_2O$ for instance, the layer distance is increased from 5.72 to about 7.04 Å (see also Table 4). This is similar to the findings of Guliants *et al.*, who incorporated ammonia (among other cations) into $VOHPO_4{\cdot}0.5H_2O$.[29]

Further heating of the resulting intermediates results in loss of the long range order ($n=2$, 4) and the subsequent formation of an amorphous phase. This is caused by the loss of crystal water and the subsequent destruction of the network of hydrogen bonds. The temperatures at which the amorphous phase is first observed (530 K for $n=2$ and 390 K for $n=4$) reflect the binding energy of the water molecules in the precursor. In the case of $VOHPO_4{\cdot}0.5H_2O$, the water molecule is so tightly bound that the loss of the water molecule does not occur until the temperature at which AVP formation starts.

A comparable reaction with ammonia was not observed when the other compounds, $VOHPO_4$ and β-$(VO)_3(PO_4)_2{\cdot}6H_2O$, were used as precursors. In the case of anhydrous $VOHPO_4$, the lack of unshared P–OH groups and its three-dimensional structure prevent easy penetration by ammonia. Instead, an oxidation process leading to isostructural β-$VOPO_4$ is observed, but not below temperatures of 630 K. In the case of β-$(VO)_3(PO_4)_2{\cdot}6H_2O$, the formation of a new phase is observed at about 470 K. It is believed that the occurrence of this phase is caused by the loss of some water molecules, probably those located within the tunnels. At temperatures above 600 K, an amorphous phase is also observed, due to further loss of water.

The formation of the final catalytically active solid proceeds *via* further intermediate phases, denoted $X2_0$ and $X2_{0.5}$. $X2_0$ was observed during the generation of AVP_{gen0}, AVP_{gen2} and AVP_{gen4} at 713 K, *ca.* 30 min after reaching the final temperature (see also Fig. 4a) for a period of about 2 h. The existence of $X2_0$ was still detected after the end of the experiment, but only in case of AVP_{gen4} formation (see also Fig. 4a). The generation of the intermediate phase $X2_{0.5}$ was detected at 713 K at the beginning of the constant temperature period during the generation of $AVP_{gen0.5}$ and AVP_{gen4} (see also Fig. 3a and 4a). In contrast to the failed attempts to prepare $X1_n$ ($n=0.5$, 2, 4) phases, the intermediate $X2_{0.5}$ was successfully synthesised by chemical means.[30] $X2_{0.5}$ shows the same composition as AVP_{syn} [α-$(NH_4)_2(VO)_3(P_2O_7)_2$] and is assumed to be the β-modification of $(NH_4)_2(VO)_3(P_2O_7)_2$. $X2_{0.5}$ crystallises in monoclinic space group $P2_1/n$ with

Table 3 Intermediate phases appearing during the generation of catalysts from different precursor compounds (temperature program: (i) heating to 393 K under air–ammonia, (ii) heating to 713 K (2.5 K min^{-1}) and kept for 5 h under a feed of the following molar ratio: toluene : ammonia : air : water vapour = 1 : 4.5 : 32 : 24)

Precursor compound	*T*/K	Intermediate phase	Final solid (crystalline proportions)
$VOHPO_4$	*ca.* 640	β-$VOPO_4$	AVP_{gen0} (AVP)
	ca. 713[a]	$X2_0$	
$VOHPO_4 \cdot 0.5H_2O$	*ca.* 390	$X1_{0.5}$ ($NH_4VOPO_4 \cdot 0.5H_2O$)	$AVP_{gen0.5}$ (AVP)[b]
	ca. 713	$X2_{0.5}$ [β-$(NH_4)_2(VO)_3(P_2O_7)_2$)][c]	
$VOHPO_4 \cdot 2H_2O$	*ca.* 360	$X1_2$ ($NH_4VOPO_4 \cdot 2H_2O$)	AVP_{gen2} (AVP)
	ca. 530	X-Ray amorphous	
	ca. 713[a]	$X2_0$	
$VOHPO_4 \cdot 4H_2O$	*ca.* 295	$X1_4$ ($NH_4VOPO_4 \cdot 4H_2O$)	AVP_{gen4} (AVP + $X2_0$)
	ca. 390	X-Ray amorphous	
	ca. 713[d]	$X2_0$	
	ca. 713[d]	$X2_{0.5}$ [β-$(NH_4)_2(VO)_3(P_2O_7)_2$][c]	
β-$(VO)_3(PO_4)_2 \cdot 6H_2O$	*ca.* 470	$X1_6$ [$(VO)_3(PO_4)_2 \cdot (6-x)H_2O$]	AVP_{gen6H} (AVP)[e]
	ca. 600	X-Ray amorphous	

[a]Observed for 2 h after reaching the final temperature. [b]An X-ray amorphous portion of V_2O_5 could be formed, as concluded from the formation of NH_4VO_3 after cooling. [c]$a = 16.9409(2)$, $b = 4.9095(7)$, $c = 9.3116(8)$ Å, $\beta = 97.159(1)°$ (calculated at r. t.).[27] [d]Appeared 30 min after reaching the final temperature. [e]VO_2, V_2O_5, V_4O_9, V_6O_{13} were also found.

Table 4 *d*-Values of intermediate phases (determined at room temperature after heating the precursor samples up to 390 ($X1_{0.5}$), 360 ($X1_2$) and 295 K ($X1_4$) and subsequent cooling to room temperature)

$X1_{0.5}$			$X1_2$			$X1_4$		
2θ/°	*d*/Å	I_{rel}	2θ/°	*d*/Å	I_{rel}	2θ/°	*d*/Å	I_{rel}
12.56	7.042	100	12.56	7.042	100	13.76	6.430	100
17.28	5.128	35	16.17	5.479	15	18.72	4.736	90
27.95	3.190	20	17.42	5.087	10	30.44	2.934	80
31.24	2.861	30	19.52	4.544	15	31.49	2.838	50
			25.23	3.527	30			
			26.63	3.344	30			
			28.29	3.152	30			
			31.14	2.870	15			
			34.75	2.580	20			

$a = 16.9409(2)$, $b = 4.9095(7)$, $c = 9.3116(8)$ Å, $\beta = 97.159(1)°$ (calculated after separation at room temperature).[31] Additionally, β-$(NH_4)_2(VO)_3(P_2O_7)_2$ seems to be isostructural with β-$K_2(VO)_3(P_2O_7)_2$[32] because the symmetry and lattice constants are very similar. The intensity of the AVP peaks constantly increased until the $X2_{0.5}$ peaks had completely vanished (after 2 h at 713 K). It is assumed that in this period the generation of the V_xO_y species proceeds, in combination with their arrangement in larger units. This behaviour is in agreement with the observation that edge-shared vanadyl octahedra running in chains or layers through the bulk enabling electronic interaction and oxygen passage are necessary and responsible for the catalytic activity in redox reactions.[33]

Significant catalytic performance for the solids (toluene conversion, benzonitrile formation) was not detected until the formation of $X2_{0.5}$ and AVP (see also Fig. 3b and 4b). Fig. 6 depicts the change in the benzonitrile yield during the generation process of $AVP_{gen0.5}$ from the intermediate β-$(NH_4)_2(VO)_3(P_2O_7)_2$. Five sections may be distinguished during the generation process. Every step is combined with a special structural composition of the generated phase: (i) only $X2_{0.5}$ can be detected as a crystalline phase after reaching the final temperature of 713 K, measurable catalytic activity can be observed and benzonitrile is formed as the selective reaction product. (ii) The phases $X2_{0.5}$ and AVP exist side-by-side, but the content of AVP increases, whereas the amount of $X2_{0.5}$ declines with time-on-stream. (iii) AVP can be detected as the sole crystalline phase. The formation of benzonitrile increases only moderately during the first five hours of the transformation process. The catalytic performance of the as-generated specimen stays rather poor at this state. (iv) Prolonging this

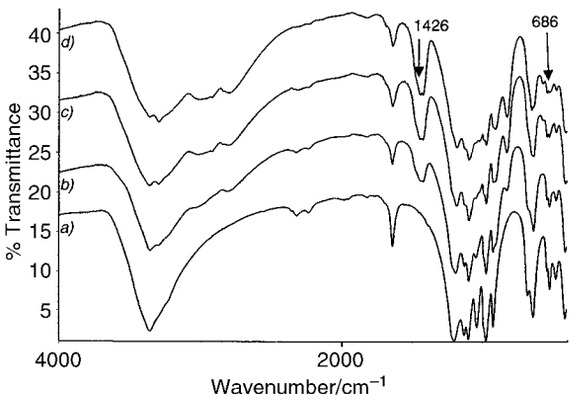

Fig. 5 FTIR spectra of $VOHPO_4 \cdot 0.5H_2O$ treated at 393 K (heating rate 10 K min^{-1}) under an air–ammonia–water vapour atmosphere for $t = 0$ (a), 30 (b), 60 (c) and 120 min (d).

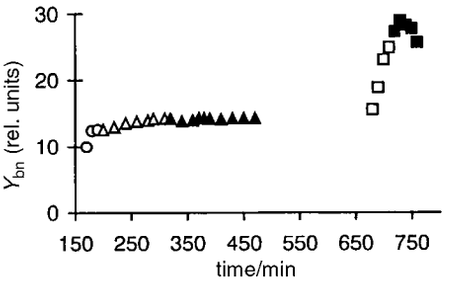

Fig. 6 Change in the benzonitrile yield (Y_{bn}) during the generation of the catalyst $AVP_{gen0.5}$ under ammoxidation conditions at 713 K: step 1 (○), $X2_{0.5}$ [β-$(NH_4)_2(VO)_3(P_2O_7)_2$]; step 2 (△), $X2_{0.5}$ + AVP [β- + α-$(NH_4)_2(VO)_3(P_2O_7)_2$]; step 3 (▲), AVP [α-$(NH_4)_2(VO)_3(P_2O_7)_2$]; step 4 (□), AVP + V_xO_y formation; step 5 (■), $AVP_{gen0.5}$.

experiment by an additional five hour period after cooling overnight results in a significant improvement of the catalytic performance. This improvement is presumably connected with the alteration of the V_xO_y structure. In a separate run, AVP_{syn} was treated under ammoxidation conditions for about 20 h at 713 K, which did not lead to further structural changes. (v) In the end, and as demonstrated in the last section, the catalytic performance is nearly constant.

The results of the *in situ* catalytic measurements obtained in the XRK reaction chamber have been compared to those obtained from a plug-flow reactor. The results obtained with the hydrogen phosphate precursor compounds are presented in Fig. 7. Comparison of *in situ* and *ex situ* measured catalytic performance shows the same tendency, besides the expected differences in the absolute values due to the differences in catalyst amount and particle size mentioned previously. It is clearly shown that the highest activity is achieved by a catalyst derived from the $VOHPO_4{\cdot}0.5H_2O$ precursor. The reasons for this are, as yet, not completely understood, since the samples AVP_{gen0}, $AVP_{gen0.5}$ and AVP_{gen2} reveal identical XRD patterns and IR spectra, as well as the same values for specific density, specific surface area (2.0–2.2 $m^2\ g^{-1}$), particle size and crystallite size. Furthermore, the H/N ratio (3.81 in AVP_{gen0} and 3.65 in $AVP_{gen0.5}$ and AVP_{gen2}),[11] which can be viewed as a measure for the ammonium ion content in contrast to other N-containing groups (*e.g.* imido or nitrido), does not explain the different activities either. Obviously, the chemical composition of the X-ray amorphous V_xO_y phase differs in the generated catalysts and, therefore, is responsible for the different catalytic results.

The EXAFS investigations reveal that the radial atomic distribution functions (RDF) of the generated catalysts are very similar with respect to the first co-ordination sphere (*ca.* 1.5–2.6 Å), but the second co-ordination sphere (*ca.* 2.6–4 Å) reveals some differences. The RDFs of AVP_{gen0} and $AVP_{gen0.5}$ demonstrate two maxima in the second co-ordination sphere, in contrast to only one broad maximum in the case of AVP_{gen2} and AVP_{gen4}. Fig. 8 depicts a comparison of the RDF of one representative of each group ($AVP_{gen0.5}$ and AVP_{gen4}) as well as of AVP_{syn}. It can be seen that AVP_{syn} shows the narrowest atom distance distribution within the first co-ordination sphere, but also the most detailed within the second. It can be reasonably supposed that a more detailed second co-ordination sphere in the RDF is a result of more regular long range ordering, as is confirmed by AVP_{syn}. This can otherwise be taken as an indication that $AVP_{gen0.5}$ (and AVP_{gen0}) contains slightly more regular long range ordering compared to AVP_{gen4} (and AVP_{gen2}) and, therefore, also probably within the precipitated V_xO_y phase. This may be seen in connection with the process of generation; AVP_{gen2} and AVP_{gen4} are formed *via* an amorphous intermediate, in contrast to AVP_{gen0} and $AVP_{gen0.5}$, which are exclusively generated *via* crystalline phases.

In order to obtain further details of the atom distribution, a fit of the measured curve to a model would be required. But this is a rather difficult venture because AVP_{syn} alone contains three crystallographically independent vanadium atoms with significant differences in the first and, especially, in the higher co-ordination spheres. Such a model would have to be superposed with that of the model V_xO_y phase, but the final result would be not reliable, since too many constraints regarding the co-ordination number and distances would have had to be introduced.

Thermal behaviour of the generated NH_4^+-vanadium phosphate catalysts

The thermal behaviour of AVP_{syn} and AVP_{gen} samples was investigated up to 1170 K in N_2 and air by XRD and TG-DTA. When AVP_{syn} or AVP_{gen} are heated above 650 K, a phase transition is observed (Fig. 9). The new phase is denoted

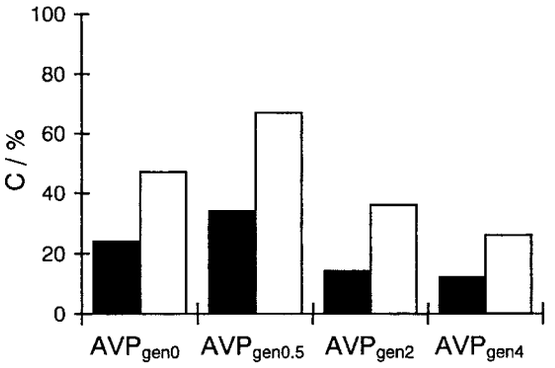

Fig. 7 Toluene conversion [*C* (%)] during ammoxidation on various AVP_{gen} samples derived from different $VOHPO_4{\cdot}nH_2O$ ($n=0$, 0.5, 2, 4) precursor phases [*in situ* XRD-monitored runs were carried out at 713 K (filled bars), catalytic tests were carried out in a plug-flow reactor at 625 K (open bars)].

as AVP′ and crystallises in the orthorhombic space group $P2_12_12_1$ with $a=17.770(1)$, $b=11.3398(7)$ and $c=6.8701(3)$ Å (Table 5). This phase transition might be connected with the liberation of ammonia and water that is observed by TG-DTA/mass spectrometer coupling at temperatures above 670 K. The decrease in the *c* parameter indicates the formation of a higher condensed oligophosphate, possibly a tetraphosphate, but there is little structural justification for such an interpretation. Complete liberation of ammonia and water could lead to the formation of either $(VO)_3P_4O_{13}$ or $V_3O_2(P_2O_7)_2$, with the latter being more likely from a structural point of view. Berndt *et al.* assume the formation of a nitrido phosphate, like $(VO)_3(P_3O_9)N$, and a polyphosphate $(VO)(PO_3)_2$.[34] AVP′ is stable up to about 810 K before it becomes X-ray amorphous. From this point, the further behaviour is different, depending on the chosen atmosphere as well as the sample (AVP_{syn} or AVP_{gen}). In an inert atmosphere, the liberation of N_2 is observed and, consequently, a partial reduction from V(IV) to V(III). This corresponds to the findings of Berndt *et al.*,[34] who followed the thermal decomposition of the nitrido phosphate phase above 973 K to $V_4(P_2O_7)_3$ [PDF 37-0073] and V_2O_3. The

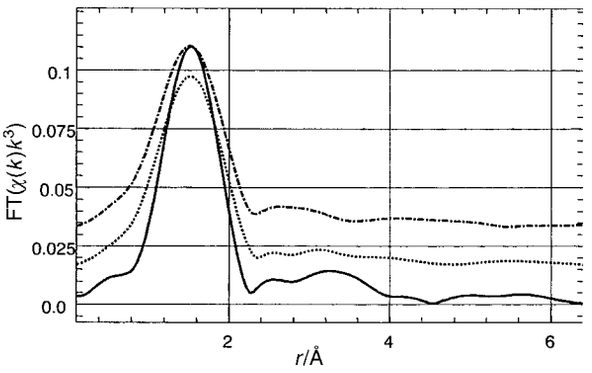

Fig. 8 EXAFS spectra (radial distribution function) of AVP_{syn} (—) compared with the spectra of $AVP_{gen0.5}$ (····) and AVP_{gen4} (·–·–).

Fig. 9 Guinier–Lenné pattern (Cu-Kα_1) of the phase transformation of AVP to AVP′ under N_2 up to 730 K ($\beta=1$ K min^{-1}).

Table 5 Crystallographic data for AVP and AVP′

	Sample	
	AVP	AVP′
Crystal class	orthorhombic	orthorhombic
Space group	*Pnam*	$P2_12_12_1$
Lattice constants/Å	17.5016	17.767
	11.3716	11.339
	7.2764	6.869

onset of N_2 liberation is decreased by about 100 K in the case of AVP_{gen} compared to AVP_{syn}.

When the samples are heated in air, the presence of oxygen prevents a reduction to V(III) and leads to recrystallisation of $(VO)_2P_2O_7$ and $(VO)(PO_3)_2$ at temperatures above 1073 K.

Conclusions

The combination of *in situ* XRD and GC analysis of the product stream during the ammoxidation of toluene on vanadium phosphate catalysts allows observation of the phase transformation of the vanadyl(IV) phosphate precursor compounds and simultaneous determination of the catalytic performance. Moreover, the catalytic performance can be attributed to the current transformation state. Crystalline vanadyl(IV) hydrogen phosphates ($VOHPO_4{\cdot}nH_2O$; $n=0$, 0.5, 2, 4) and the vanadyl(IV) mono phosphate β-$(VO)_3(PO_4)_2{\cdot}6H_2O$ were used as precursor compounds and were transformed into vanadium oxide-containing ammonium vanadyl(IV) pyrophosphate. During the transformation process two different groups of crystalline layered ammonium vanadium phosphates are generated as successive intermediate phases: (i) $NH_4VOPO_4{\cdot}nH_2O$, $n=0.5$, 2, 4 and (ii) β-$(NH_4)_2(VO)_3(P_2O_7)_2$. Layered β-$(NH_4)_2(VO)_3(P_2O_7)_2$ is further transformed into distorted α-$(NH_4)_2(VO)_3(P_2O_7)_2$ showing a network structure. The formation of α-$(NH_4)_2(VO)_3(P_2O_7)_2$ is accompanied by the generation of V_xO_y species from the vanadium surplus. Measurable catalytic activity is connected with the formation of β-$(NH_4)_2(VO)_3(P_2O_7)_2$ and various vanadium oxides. The structure of the precursor compound is responsible for the particular pathway followed in generating the catalyst and, in particular, for the formation, the proportion and the valence state of the V_xO_y species.

Acknowledgements

The authors thank Dr D. Schultze (BAM—Bundesanstalt für Materialforschung und -prüfung, Berlin, Germany) for thermal analysis, Mrs U. Wolf for the FTIR measurements and Mrs W. Winkler for experimental assistance. Financial support by the Deutsche Forschungsgemeinschaft (grant no. Ste 692/5) is gratefully acknowledged.

References

1 G. Centi, *Catal. Today*, 1993, **16**, 5.
2 G. Hutchings, *Appl. Catal.*, 1991, **72**, 1.
3 E. Bordes, *Catal. Today*, 1987, **1**, 499.
4 C. C. Torardi, Z. G. Li, H. S. Horowitz, W. Liang and M. H. Wangbo, *J. Solid State Chem.*, 1995, **119**, 349.
5 A. Martin and B. Lücke, *Catal. Today*, 2000, **57**, 61.
6 I. Matsuura, *Stud. Surf. Sci. Catal.*, 1992, **72**, 247.
7 A. Martin, H. Berndt, B. Lücke and M. Meisel, *Top. Catal.*, 1996, **3**, 377.
8 A. Martin, B. Lücke, H. Seeboth, G. Ladwig and E. Fischer, *React. Kinet. Catal. Lett.*, 1989, **38**, 33.
9 A. Martin, U. Steinike, K. Melanova and V. Zima, *J. Mater. Chem.*, 1999, **9**, 2523.
10 Y. Zhang, A. Martin, G. Wolf, S. Rabe, H. Worzala, B. Lücke, M. Meisel and K. Witke, *Chem. Mater.*, 1996, **8**, 1135.
11 U. Steinike, F. Krumeich, L. Wilde, A. Martin and G.-U. Wolf, *Mater. Sci. Forum*, 1998, **278–281**, 660.
12 A. Martin, G.-U. Wolf, U. Steinike and B. Lücke, *J. Chem. Soc., Faraday Trans.*, 1998, **94**, 2227.
13 A. Martin, U. Steinike, S. Rabe, B. Lücke and F. K. Hannour, *J. Chem. Soc., Faraday Trans.*, 1997, **93**, 3855.
14 L. Wilde, H. Worzala, U. Steinike and G.-U. Wolf, *Mater. Sci. Forum*, 2000, **321–324**, 982.
15 R. G. Rizayev, E. A. Mamedov, V. P. Vislovskii and V. E. Sheinin, *Appl. Catal. A*, 1992, **83**, 103.
16 R. K. Grasselli and J. D. Burrington, *Adv. Catal.*, 1980, **30**, 133.
17 Y. Zhang, M. Meisel, A. Martin, B. Lücke, K. Witke and K.-W. Brzezinka, *Chem. Mater.*, 1997, **9**, 1086.
18 R. A. van Santen, *Handbook of Heterogeneous Catalysis*, ed. G. Ertl, H. Knözinger and J. Weitkamp, Wiley-VCH, Weinheim, 1997, vol. 5, p. 2244.
19 E. Bordes, *Elementary Reaction Steps in Heterogeneous Catalysis*, ed. R. W. Joyner and R.A. van Santen, Kluwer Academic Press, Amsterdam, 1993, p. 137.
20 J. W. Niemantsverdriet, *Spectroscopy in Catalysis*, VCH, Weinheim, 1993.
21 D. Fratzky, T. Götze, H. Worzala and M. Meisel, *Mater. Res. Bull.*, 1998, **33**, 635.
22 J. Freiberg, N. Wüstneck, H. Wolf and G. Ladwig, *Z. Anorg. Allg. Chem.*, 1985, **527**, 62.
23 M. E. Leonowicz, J. W. Johnson, J. F. Brody, H. F. Shannon, Jr. and J. M. Newsam, *J. Solid State Chem.*, 1985, **56**, 370.
24 A. LeBail, G. Ferey, P. Amoros and D. Beltran-Porter, *Eur. J. Solid State Inorg. Chem.*, 1989, **26**, 419.
25 L. Wilde, J. Trommer, U. Steinike, H. Worzala and G.-U. Wolf, *Mater. Sci. Forum*, 1998, **278–281**, 704.
26 R. Gopal and C. Calvo, *J. Solid State Chem.*, 1965, **338**, 266.
27 L. Wilde, Ph.D. Thesis, Humboldt-Universität zu Berlin, Berlin, 2000.
28 G. Mosel, personal communication.
29 V. V. Guliants, J. B. Benziger and S. Sundaresan, *Chem. Mater.*, 1994, **6**, 353.
30 S. Rabe, personal communication.
31 L. Wilde, U. Steinike, A. Martin, M. Fait and B. Müller, *Mater. Sci. Forum*, in press.
32 K. H. Lii, H. J. Tsai and S. L. Wang, *J. Solid State Chem.*, 1990, **87**, 396.
33 A. Brückner, A. Martin, B. Lücke and F. K. Hannour, *Stud. Surf. Sci. Catal.*, 1997, **110**, 919.
34 H. Berndt, K. Büker, A. Martin, S. Rabe, Y. Zhang and M. Meisel, *Catal. Today*, 1996, **32**, 285.